Solar diameter, transits and Limb Darkening at the Clementine Meridian Line

Andrea Radano
Riccardo Iafrate

23 September 2026

Abstract

This work reports the main results of the laboratory experiences at the Basilica of Santa Maria degli Angeli e dei Martiri at Piazza della Repubblica in Rome, carried out under the supervision of professor Costantino Sigismondi. During the last semester, several measurements were taken in different contexts, such as: solar diameter, transit times, Limb Darkening profiles (LDP), eclipse simulations by sunset, stellar transits and noise measurements of local seeing.
Here, only the main laboratory activities of the semester will be reported, represented by the discrepancies between the ephemerides and the data collected on the position of the center of the image, the solar diameter and the transit times. There is also a comparison between the LDPs measured at the Basilica and Rogerson's data. Finally, there will also be a brief mention of the measurement of the power spectra of seeing and its correlation with temperature and position in the solar ellipse.

1 Introduction

The Basilica of Santa Maria degli Angeli e dei Martiri represents a bridge between religion, arts and science. Built during the pontificate of Pope Clement XI in 1701-1702, the Clementine Gnomon, still present in the basilica today, was designed to measure parameters of the Earth's orbital motion and to verify the accuracy of the Gregorian calendar reform. Those parameters were obliquity, eccentricity of the ecliptic and the duration of a tropical year ([[2]]). Today, the meridian line is still used for scientific purposes, in particular for measuring the diameter of the sun, both through measurements solar diameters and transits.

1.1 Importance of solar physics

Because the Sun is relatively close compared to other stars, it is possible to observe significantly more detail on its surface.

One of the Sun's features that has been observed and analyzed in this study is the Limb Darkening profile of the Sun. The LDP is defined as the intensity I of the Sun on the equatorial axis as a function of the distance from the center of the star or as a function of the angle between the points, the center of the star and the detector.
This phenomenon is related to the solar atmosphere: since the temperature decrease if the distance from the center of the Sun grows, it means that measuring the intensity at the center of the Sun means observing deeper in the atmosphere and so higher temperature, and the opposite for the limb.
Also from modern observation it was shown that convection plays an important role in energy transport and in particular the ions and the H_2 molecules contributes to the characteristic LDP through the opacity([[3]]).

2 Experimental set up

The Clementine Gnomon of Francesco Bianchini is a camera obscura where the light is propagated through a pinhole of 2.5 mm of diameter and 6.22 mm of depth. The light cone is projected on the meridian line, composed of brass plates approximately 3.2 cm thick, arranged in series next to one another, forming a line of 44.89 m oriented on the North-South direction. On this line, multiples of a standard unit (1/100 of the height of the pinhole above the west side) are indicated, along with their conversion to the corresponding angle between that point and the pinhole.
Here is reported the conversion formula from a generic d, number of standard unit, to angles (zenith distance):

$$z = tan^{-1}\left(\frac{d}{100}\right) \tag{1}$$

Knowing all these information about the peculiarities of this apparatus, it was possible to obtain very precise observations, including star transits during the day. There were also portable graduated rulers made of brass which were probably used to interpolate the position of the transits along the meridian line, increasing the precision of the measurements.



Figure 1: Ruler used to measure solar and stellar transits. Located on the right respect to the main altar of the church.

At present, the level of precision achieved in the past is no longer accessible due to the deterioration of the brass line, which has resulted in the loss of all its markings, but it is possible to compensate and increase the precision using low-cost technology, such as smartphone cameras to record transits and LDP from indirect measurements or a photodiode connected with Arduino UNO to do noise measures on the LDP in order to study its properties and its spectrum. Today the main sources of uncertainty are local seeing, which contributes to turbulences on the solar image, a scaling error due to misalignment between the point on the meridian line and the point used as reference along the meridian line and of course weather conditions during the transit.

3 Methodology of measurements

In this work, the errors due to indirect measurements were computed using the following relation:

$$\sigma_y = \sqrt{\sum_{i,j} \frac{\partial y}{\partial x_i} \frac{\partial y}{\partial x_j} Cov(x_j, x_i)} \quad y = y(x_1, x_2, ..., x_n), \tag{2}$$

in our case all the measures were independent so all the off-diagonal terms vanish.

3.1 Meridian transit

The solar diameter was measured via direct measurements during transits on the meridian line and the Carrara's white marble with the supervision of Professor Costantino Sigismondi. Both transit time measurements and position measurements of the projected solar image on the meridian line were carried out. The measurements were mainly taken during the period between February and the end of March of this year. The observations of the meridian transit were possible, weather permitting, during the passage of the solar image across

the white marble.
For what concerns spacial measurements, the distances between the northern limb (closer to the pinhole) and southern limb (farther from the pinhole) of the Solar image projected on the meridian line were measured, which correspond to the major axis of the solar ellipse. During the daily transit, the positions of the limbs were marked on the white marble and on the meridian brass line using a pencil, then the distances were measured using a measuring tape. Once the position measurements were completed, a manual fit was made to match the collected data for each limb. Finally, their relative distance and their distances with respect to the nearest reference point were taken, whose distance with respect to the pinhole is known with high precision. In this way, it was possible to determine the position of the image limbs and then the center of the image along the meridian.
Regarding the time measurements, the parallel transits method was used, meaning the transit time measurements were taken, corresponding to the instant at which the center of the solar image, moving in the West-East direction, overlaps with the longitudinal axis of the meridian line. During the measurements, both the contact times with the meridian line and those with the edges of the white marble were considered: these times were averaged to estimate the meridian transit time with greater precision. To obtain these measurements, videos of the transits were made using smartphone cameras, which initially recorded a Casio G-SHOCK digital watch to provide a reference time to obtain more precise contact times with the brass line and white marble.

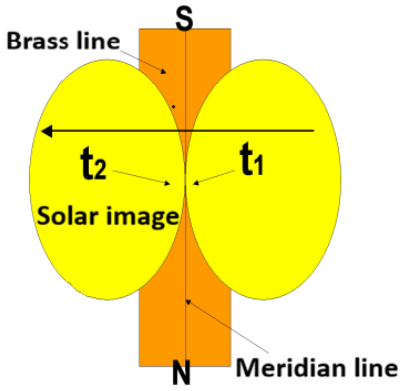


Figure 2: Contact scheme considered during all the measurements of meridian transit (adapted from [[2]]).

3.2 Limb Darkening

The Limb Darkening profile was obtained from video recordings using the drift scan technique, which consists of using a camera, in this case of the smartphone, properly aligned along the line of sight of the pinhole still on the equatorial axis

of the solar disk and recording the transit on the camera. This one was set up in "video pro" mode, when it was possible (always except for the video "21/02-2"), using ISO=50 and exposition time $t_{exp} = 1/6000s$ to maximize the contrast between the light of the Sun and the background. Since the Sun was moving in the sky, and then the solar ellipse too, the measurement of the diameter of the solar light in time was equivalent to a spatial measurement of intensity.
It was assumed that the solar disk moved along a straight line during the realization of the video. In general it's not true but for short distances can be a good approximation.
For this analysis, all frames within a given time domain range were analyzed, measuring the radius from 360 different directions and computing, from those radii, the expected value and its standard deviation. The effect of the local seeing on the received signal was neglected, mainly because, with a frequency of 30 Hz, it was not possible to correctly identify the frequencies in the Fourier space due to the aliasing. It is important to recall that the acquisition rate of a camera is 30 Hz, half of the maximum frequency perceivable from a human eye.

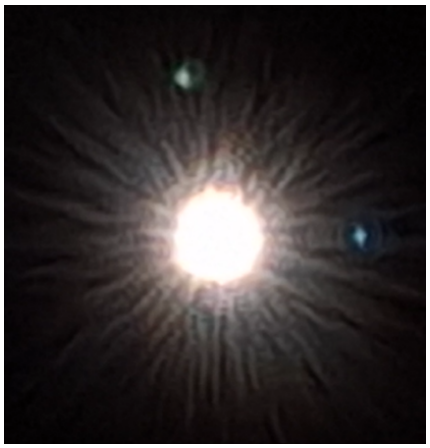


Figure 3: The image shows the calibration window for the video taken on 21/02-1 at the end of the calibration with 2 ghost images one on the right and the other on the upper side of the circle.

3.3 Photodiode measurements

In order to study the local seeing power spectra, a photodiode IPL 10530DAL was used, the same one used in Battistelli's astrophysics laboratory, connected to Arduino UNO, which was connected to a computer. The whole apparatus was placed on the floor of the Basilica and, using the "copy" tool of Arduino, all the data were saved to files. For all the measurements done, no delay was used, in order to have the maximum spectral range possible. In fact, the characteristic time of the photodiode was of the order of $\sim 10\mu s$, whereas Arduino's clock has a period of 1 ms. During the measurements, the intensity value and the corre-

sponding time were saved. The temperature T during the measurements was also recorded, using Meteo Blue temperature maps, which provide temperature maps for the whole city [5].

4 Data Analysis

4.1 Meridian transits

For the data analysis of transit times, all the video recordings made with the smartphones were carefully watched with the Google Vids software, which allows videos to be analyzed frame by frame, offering a precision of a tenth of a second. At the beginning and at the ending of the videos, when it was possible, the watch was framed, providing a real time reference to be taken into account while reviewing the video. In the absence of the watch, the video details, provided by the smartphone used for the recording, were used to obtain the video's end time, to be used as a time reference. For each transit, the times of first (t_1) and last (t_2) contact of the solar ellipse with the meridian line (as shown in the figure 2), the time at which the major axis is aligned with the center of the meridian line (t_c) and the first (t_e) and last (t_u) contact with the white marble (respectively t_e and t_u) were taken. The means between t_1 and t_2 and also between t_e and t_u were computed. Then, these results were also averaged with t_c in order to obtain the best estimate of the meridian transit time.



(a) Instant of entry in the white marble (t_e).

(b) Instant of first contact with the meridian line (t_1).

(c) Instant of the meridian transit (t_c).

(d) Instant of second contact with the meridian line (t_2).

(e) Instant of exit from the white marble (t_u).

Figure 4: Example of a meridian transit observed on 23/03, following the contact scheme in fig 2.

For each meridian transit, an Excel spreadsheet was compiled with the observational data. An example is reported in the image below:

METEO/T/P/umidità	GIORNO	MESE	ANNO	TRANSITO	EFFEMERIDI	CENTRO SOLE[°] -/+ ATM	PARAMETRI IMMAGINE
METAR LIRU 231050Z 34003KT 260V040 C	23	3	2026	12:16:49.3	12:16:33.5	49,2228	arcsec/mm img reale
METAR LIRU 231150Z 31005KT 290V360 ş	sereno	16	1013	45	Offset lembi [- =vs CNC]	49,2371	5,8114
BORDO NORD th- vs CANCRO	49,504	17372,7	equinozio	-884,0	-0,91	DIAM SOLE ' / "	diam. Teorico
BORDO SUD th-vs CAPRICORNO	48,970	17723,7	equinozio	-533,0	-0,62	32,0947	350,7
ΔT teorico	16,2	DEMPTA PEN+C	OMBRA SUD mm	5,36	parti cent. dempta pen.	1925,68	diam. Misurato
velocità immagine mm/s	2,002	17379,8	shit del centro c	2,68	85,3902		351,0
lunghezza dempta	331,4	17711,2	FORO meridiano eff.	19,64	87,0182		O-C (diametro)
ΔToss/seno nullo	15,8	-0,392	Offset centro img	-0,76	86,2042	diam. -5.3±2.6 mm	0,3

Figure 5: Example of an Excel spreadsheet filled with the observation values and those automatically computed on 23/03. The same procedure was used for all the days on which the measurements were taken.

The spreadsheet contains a section dedicated to entering the daily weather data (humidity percentage, pressure and temperature) provided by the METAR website for the Roma Urbe airport. Then, in the dedicated cell, the transit time observed from the videos (orange cell) was entered. To fill in the ephemerides cells, the Stellarium software version 0.20.2. was used. In order to study the parameters of interest, the atmospheric contribution was removed through the software settings and the observed transit time was entered.
With this configuration, the parameters of altitude, azimuth and apparent solar diameter were observed. For what concerns the ephemerides transit time, the value corresponding to an azimuth of 180° was considered,which is the time that would be observed if the meridian line were oriented exactly in the North-South direction. After entering all these values, the Excel spreadsheet automatically calculates the theoretical diameter of the solar image and the position of the Sun even in the presence of atmosphere, obtained by considering the Cassini correction.
For the solar image diameters, repeated measurements were taken during the entire transit. Both the positions of the Northern and Southern limb with respect to the reference points and also for the direct measurements of diameters, an instrumental uncertainty of ± 0.3 mm, associated with the measuring tape, was considered. Furthermore the standard deviation was also computed for the diameters, which, when added in quadrature, makes the contribution of the instrumental uncertainty negligible.
For the uncertainty on the positions of the limbs with respect to the considered reference points, used to determine the center of the solar image, in addition to the instrumental contribution, a scale error, due to a misalignment along the longitudinal axis of the meridian line between the reference points and fits, was considered.
After compiling the Excel spreadsheet, it was possible to compare the values observed during measurements with the values computed from the Stellarium ephemerides for the position of the Sun's center, the solar diameter and the meridian transit time.
Giandomenico Cassini (1625-1712) became famous for his evaluation of the effect of atmospheric refraction on the apparent position of an object in the sky, which optically 'raises' the observed object the closer it is to the horizon. The Cassini correction (c) ([[1]]), valid up to a zenith distance of z=75° is given by the following formula:

$$c = 60'' \cdot \tan(z), \tag{3}$$

from which it's possible to obtain:

$$z_{vero} = z_{oss} + c, \tag{4}$$

where z_{vero} is the corrected value of z, while z_{oss} is the observed value.
In order to compute z, the eq. 1 was used. The altitude of the Sun (h) is obtained from the following relation:

$$h = 90° - z. \tag{5}$$

To convert h from degrees to the corresponding distance (in mm) of the center of the solar image ($h[mm]$) from the foot of the pinhole, the following formula was used:

$$h[mm] = \frac{H[mm]}{\tan(h[°])}, \tag{6}$$

where H=20353.44 mm is the height of the pinhole.
Regarding the center of the Sun, the differences between the observed position and the one obtained from the Stellarium ephemerides in the presence of the atmosphere were calculated (using the equations(5-6)). These differences are shown in the following graph:

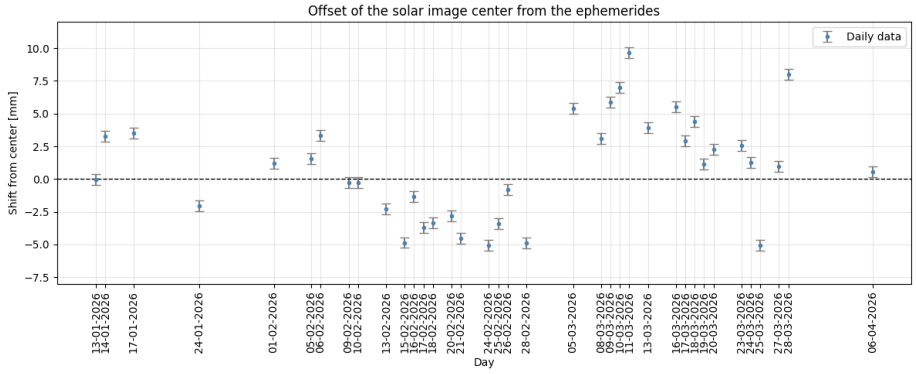


Figure 6: The graph shows the differences in the center positions, with the corresponding uncertainties, for the different days considered.

The graph shows an oscillatory trend in the center offset, highlighted by the transition from negative values in February to positive values in March. This trend may indicate that the brass line is not perfectly straight, but rather has small deviations on the millimeter scale.
For the diameters, the differences between the observed diameter and calculated (from ephemerides) values (O-C) were calculated and reported in the graph below:

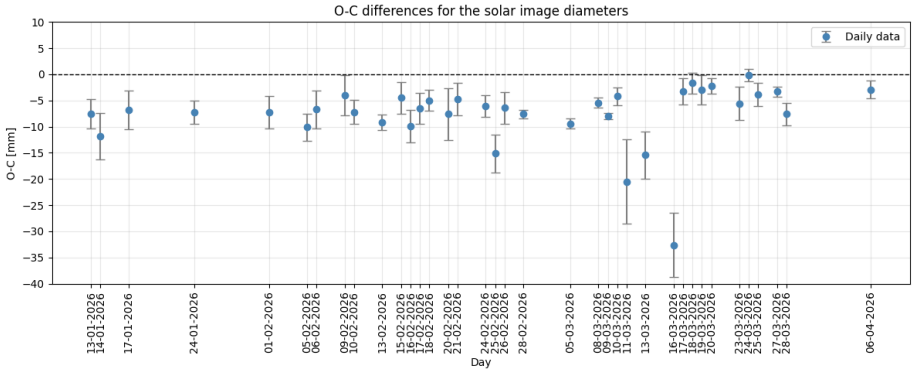


Figure 7: The graph shows the differences between observed and calculated theoretical diameters (O-C), with the corresponding uncertainties, for the different days considered.

From the graph, it can be observed that, in the period between January and early March, there is a systematic underestimation of the diameter of about 5 mm: this could be due to the reflectance of the white marble, which in the winter months makes the edge of the solar image less identifiable. In particular, on March 11, 13 and 16, the (O-C) deviation from zero appears larger, probably because these three measurements were taken by a different student than usual. From March 17 onward, as the spring equinox approaches, the deviation decreases, since the size of the solar image decreases and its brightness increases, thus increasing the contrast between the floor and the image, allowing the edge of the image to be distinguished with greater precision.
By calculating the difference between the observed transit time and the transit time given by the ephemerides, the delay (Δt_{oss}) of the real meridian line with respect to an ideal meridian line was determined.
In order to decrease the uncertainties on the time measurements, the video recordings were watched frame by frame with a fixed time reference given by the Casio or the smartphone. The contribution considered are due to the resolution of the video player, which contributes with an error of about $\pm(1/\sqrt{12})$ s, and to the analysis of the single frame, which contributes with an error of about $\pm(1/30)$ s. Adding in quadrature, a total uncertainty on times of ± 0.3 s was obtained. Here is reported the delay Δt_{oss} for the different days considered:

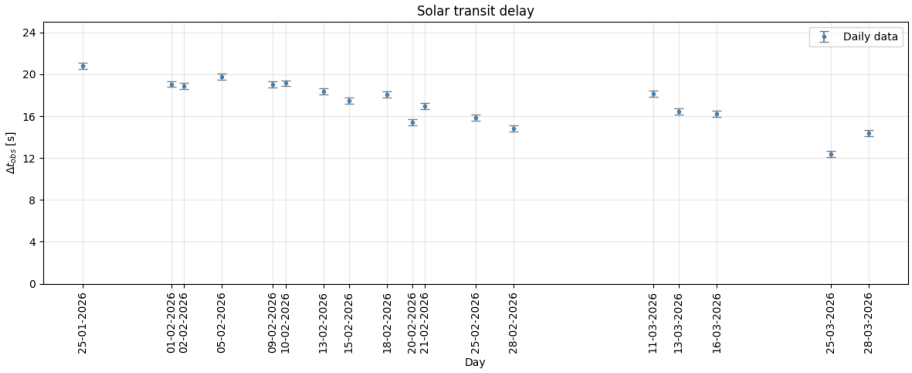


Figure 8: The graph shows the transit delays, with the corresponding uncertainties, for different days.

From the graph, it's easy to see that the delay between the observed transit and the one predicted by the ephemerides is always present. A generally decreasing trend can be observed, from approximately 20 s of delay in January to the decrease observed as the spring equinox approaches.The small oscillations around the overall trend could be due to minor millimetric misalignments of the brass line or statistical fluctuations.

4.2 Limb Darkening

Using python libraries such as numpy, cv2, matplotlib, it was possible to analyze every frame of the previously recorded videos to find the radius of the circle over time to obtain the Limb Darkening profile as a function of time. To do so, a dictionary was defined, containing all the input and output variables of the data analysis: $VIDEO_PATH$ which is the video's name, $PREVIEW_FRAME$ identifies the frame used for calibration, from which $CENTER_X$ and $CENTER_Y$, that corresponds to the center of the circle, are determined, $PROFILE_ANGLE$ is the angle, $WINDOW_HALF_SIZE$ corresponds to the half of the length of a square centered around the center of the circle to save only the pixels inside the square in every frame, $FRAME_START$ and $FRAME_END$ which correspond to the first and last frame to analyze, R_{MAX} and R_{MIN} which are the extremes of the radial distance range in which the intensity radial profiles were measured, N_{ANGLES} is the number of directions measured along the radial profiles, $FRAME_STEP$ is the number of frames between two consecutive analyzed frames, at the end it was always 1 but during preliminary analysis its value was raised to have faster analysis, $INTENSITY_MODE$ is the metric which compresses the 3 channels of the video into one and it was always set in RGB_mean that corresponds to the arithmetic mean of the channels in every pixel, $EXPORT_CSV$ is just a setting used to save the final results of the analysis in .csv files, $GRADIENT_EPSILON$ is the tolerance on the first derivative of the ra-

dial profiles and it allows to have a criterion to find the radius, then we have $MIN_CONSECUTIVE$ which is the minimum number of pixels that satisfy the criterion of the radius, also called as MNP, it was adopted to avoid noise. In the second paragraph of the cell there are represented all the default settings for plots during the calibration: the size of the picture, the size of data points, a square for the window, $SHOW_RADII$ to represent a circle of radius $R = R_{MAX}$, the center of the circle, all on the preview frame, and another plot with the radius computed using the $\epsilon - criterion$ radius compared with the radius found searching for the maximum variation of intensity along the radial direction, all as a function of angle. In the end because of its instability the maximum derivative criterion wasn't used.

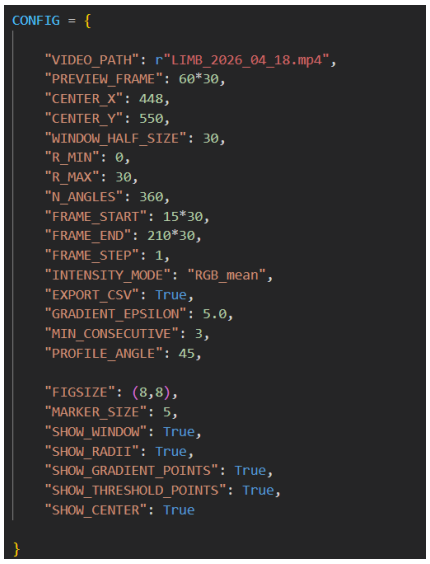


Figure 9: The image shows the dictionary used for the data analysis of the Limb Darkening.

After that, a frame was chosen as "$PREVIEW_FRAME$" such that the apparent diameter of the solar image was approximately maximum, in order to find the geometric center of the circle and its maximum extension and the three colour channels were compressed into one with the arithmetic mean of the channels for every pixel. The center was found by tuning the parameters until the error on the barycenter was less than one pixel.
After that, the following tools were tuned: $WINDOW_HALF_SIZE$, R_{MAX}, $FRAME_START$ and $FRAME_END$ were tuned watching the video in order to analyze only the frames where it was observed the Solar light on the camera.
Once all these parameters were tuned, "$clear_output$" from
Iphyton.display was used to generate a dynamic plot in which, every 0.1 seconds, the radial intensity profile at a fixed angle was overlaid, enabling us to

tune the tolerance parameter ϵ and MNP.
A table with all the calibration variables used, along with the corresponding video, is reported here:

Day	21/02-1	21/02-2	25/02	23/03	18/04
(X_C, Y_C) [px]	(1004,590)	(540,880)	(688,900)	(411,769)	(448,550)
$PREVIEW_FRAME[]$	6000	5400	3300	3000	1800
$WINDOW_SIZE$ [px]	200	600	50	50	60
ϵ [bit/px]	5	1	5	5	5
MNP [ ]	3	3	3	3	3

Table 1: The table reports the calibration variables used for each analyzed video.

It's important to explain that, strictly speaking, imposing a tolerance on the first derivative is not an entirely rigorous way of determining the radius. However, since the contrast was high and the camera was almost always saturated by sunlight over most of the circle's extension, the first derivative inside the circle was nearly zero, with a sharp increase in its modulus at the boundary.
After the calibration, the analysis was extended to all frames within the time domain window for all videos acquired during the semester. For each frame, the radius was computed along 360 different directions, one for each degree and then the corresponding expected value and standard deviation were computed. The radius was defined in the following way:

$$r =< distance(I^*) >_{MPN}, \tag{7}$$

where I^* is such that $|\left(\frac{dI}{dr}\right)_{\theta=cost, I=I^*}| > \epsilon$.
Because of the high contrast of the videos, the difference between the frames taken from different channels was approximately the same. For this reason the intensity I was defined using the following relation:

$$I = \frac{R+G+B}{3}, \tag{8}$$

where R, G, and B are the three channels of the videos.
It's important to clarify that, since all the pixel coordinates has integer values, a linear interpolation was used, weighted based on the distance between the pixel coordinates and the radial distance of interest, to extrapolate the intensity at integer radial distances from the center of the circle for directions other than 0, 90, 180 270 degrees.
Once the radii and their errors were obtained, the LDPs were normalized to 1 by dividing by their maximum. Here is reported the propagation formula used:

$$\sigma_{I\,norm,i} = (1-\delta_{i,max})\sqrt{\left(\frac{\sigma_{I_i}}{I_{max}}\right)^2 + \left(\frac{I_i \sigma_{I_{max}}}{I_{max}^2}\right)^2} \tag{9}$$

Here is shown one of the profiles obtained using the procedure explained above:

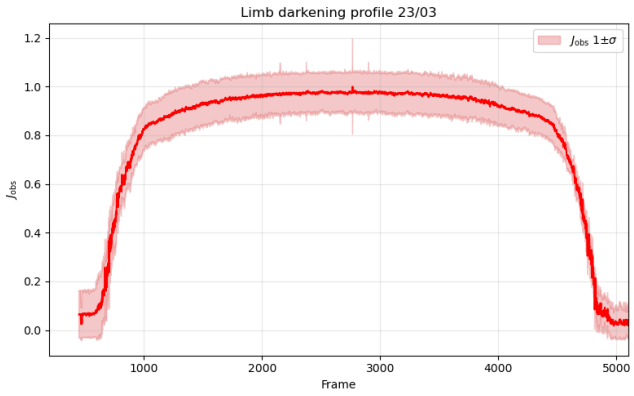


Figure 10: The graph shows the Limb Darkening normalized profile in the frame domain.

As can be seen from this picture and from the Limb Darkening profile, the criterion used shows their limits when the intensity is bigger than 80% of the central intensity, due to deviations from circularity caused by the camera's response to saturation from sunlight. In principle the precision of this measurements can be increased simply by better tuning the directions used for the computation of the expected value and its standard deviation or by changing the criterion to check only the intensity values, using the fact that at the center of the circle the camera is saturated. In reality, this doesn't matter for our purpose, because the Princeton-Michigan universities' data has an intensity range smaller than 80% of the central intensity. Moreover it's possible to distinguish also small asymmetries between right and left tails because of the small misalignment between the major axis of the Solar image and the meridian line passing through passing through the camera.
After that, all the profiles were compared with the Limb Darkening profile of ([[1]]).
In order to properly compare the data, the radius of the Sun was found as the inflection point of the profile ([[4]]), then the profile was shifted and rescaled to the radius of the Sun.
Here is a plot of Rogerson's data:

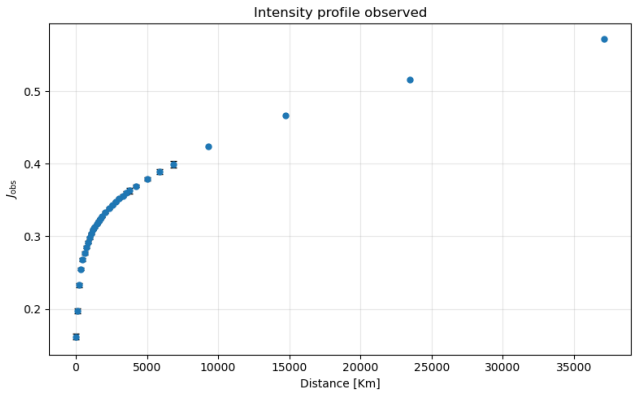


Figure 11: The graph shows the Limb Darkening profile measured by ([[1]]), expressed in terms of its central intensity as a function of kilometers.

Below is shown the comparison with one of the profiles obtained experimentally preserving the proportions of Figure 10:

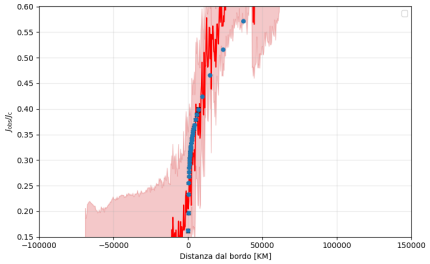


Figure 12: Comparison of the Limb Darkening profile measured on 21/02 left tail.

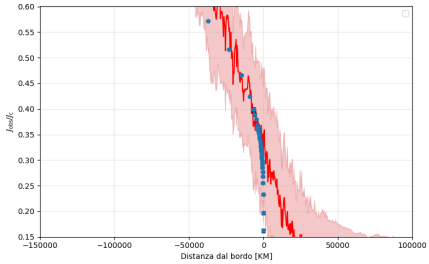


Figure 13: Comparison of the Limb Darkening profile measured on 21/02 right tail.

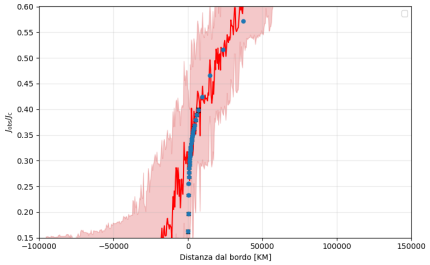


Figure 14: Comparison of the Limb Darkening profile measured on 25/02 left tail.

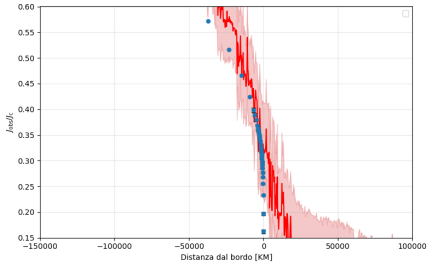


Figure 15: Comparison of the Limb Darkening profile measured on 25/02 right tail.

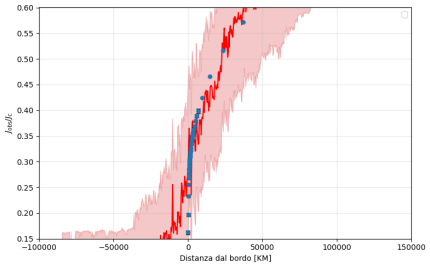


Figure 16: Comparison of the Limb Darkening profile measured on 23/03 left tail.

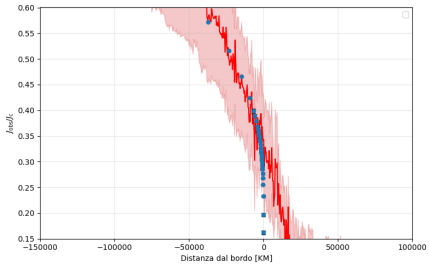


Figure 17: Comparison of the Limb Darkening profile measured on 23/03 right tail.

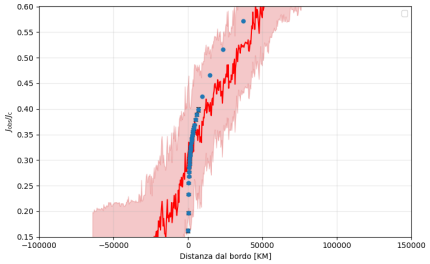


Figure 18: Comparison of the Limb Darkening profile measured on 18/04 left tail.

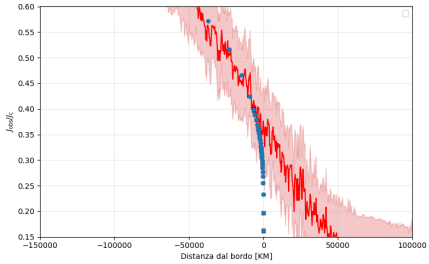


Figure 19: Comparison of the Limb Darkening profile measured on 18/04 right tail.

It is possible to see that the data are in good agreement with the Princeton-Michigan data. Of course, the difference becomes progressively larger approaching the radius of the Sun. This behaviour is due to the different kind of measurements and the role of the atmosphere in these experiments. In fact, Rogerson's experiment used an atmospheric balloon to obtain a direct measurement of the LDF, whereas our measurement was a drift scan measure and then a time-domain experiments converted in space domain assuming a constant velocity and a straight trajectory throughout the experiment, and was therefore an indirect measurement. Moreover, since our measurement was a ground-based experiment, the role of the atmosphere is more important and this becomes evident at $d = 0$ km, where the LDF measured continues for distances from the center of the sun greater then the radius of the Sun. In the end it's important to consider the fact that the LDF is convoluted with the point spread function of the pinhole and its effect is more important near the Solar radius.

4.3 Photodiode measurements

The photodiode, connected to the Arduino and to the computer, was placed on the floor of the basilica, at the point corresponding to the passage of the solar image during the meridian transit, positioning it at specific locations. To avoid fluctuations during data acquisition, due for example to the movements of the apparatus, interactions with the computer were minimized, limiting them only to saving the data.
The photodiode measurements were carried out on seven different days, performing multiple data acquisitions on the same day at specific positions, using the drift scan technique, in order to verify the dependence of the atmospheric seeing spectrum on temperature and position. These measurements were carried out with reference to the study conducted by Professor Jörn Sesterhenn from the University of Bayreuth in Germany. He tried to verify if different intensity values could be observed at different positions of the solar image, in order to understand whether the atmospheric turbulence was in phase or not.
After obtaining the data, it was possible to compute all the measured data spectra defined as the modulus of the Fourier Transform, along with their corresponding uncertainties, using FFT algorithms. Here the propagation formula on the FFT is reported:

$$\sigma_{|A_n|} = \sqrt{\sum_{k=0}^{N-1} \left(\frac{Re(A_k)\cos(\frac{2\pi}{N}kn) - Im(A_k)\sin(\frac{2\pi}{N}kn)}{|A_k|} \right)^2 \sigma_{V_k}^2}, \tag{10}$$

where A_k are the single amplitude of the Fourier Transform and N are the number of components of the intensity array measured V. Assuming that the spectra obtained follow the trend of a power law, fits were done using a law of the type:

$$y = a \cdot x^b + c, \tag{11}$$

where a is the amplitude, b is the exponent and c is a constant. From the fits, the values of a, b and c were obtained, along with their corresponding uncertainties, focusing in particular on the values of b.
After obtaining the values of b for a specific day, these were averaged and the sample standard deviation was associated whit the averages as the uncertainty. The means of b as a function of temperature T, taken from [5] for the individual days are reported in the following graph:

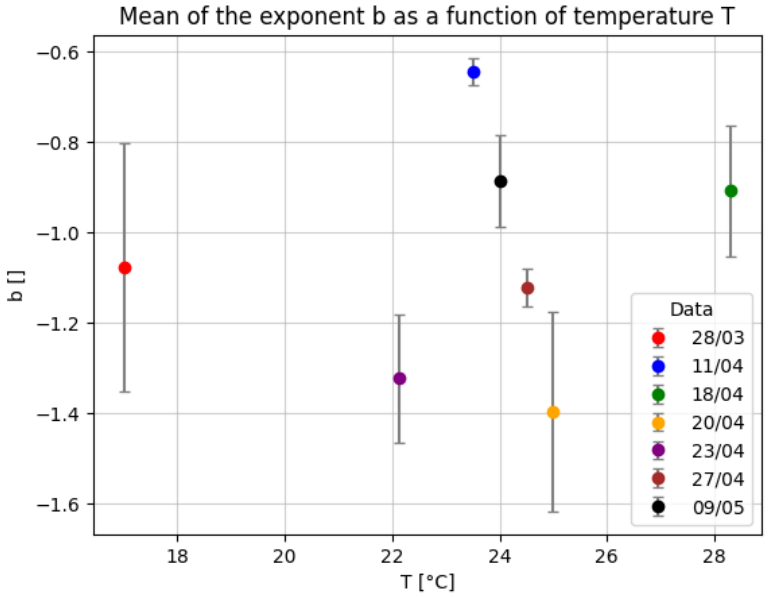


Figure 20: The graph shows the means of the exponent, with the corresponding uncertainties, as a function of temperature for the different days considered.

To study the type of dependence of b on temperature, two different types of fit were done: a linear one and a constant one. From the analysis, chi-square (χ^2) values of 99.51 (19.9 reduced) and of 108.79 (18.13 reduced) were obtained, respectively, for the linear fit and the constant one. The high χ^2 values for both models make it possible to rule out a linear and a constant relationship with temperature.
For each day, different positions of the photodiode were chosen during data acquisition. Then, the values of b were averaged for a specific position on the solar ellipse, to which an uncertainty equal to the sample standard deviation was associated. After that, the means as a function of position are reported in the graph below. The chosen positions are the northern limb, the Northern Tropic, the equator, the Southern Tropic and the southern limb of the solar ellipse, respectively indicated as -2, -1,0, 1, 2 in the graph.

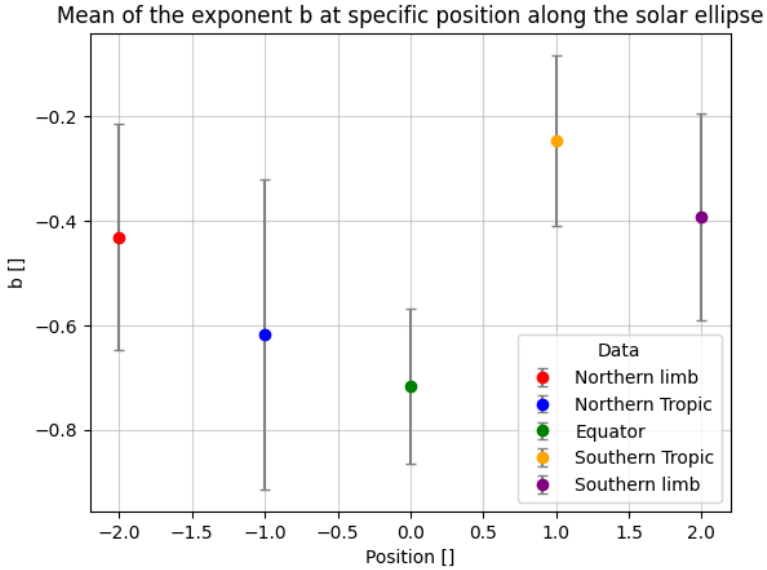


Figure 21: The graph shows the means of the exponent, with the corresponding uncertainties, as a function of the position on the solar ellipse.

As done previously, to study the dependence of b on position along the solar ellipse, a linear fit and a constant fit were done. In this case, the χ^2 values are 4.31 (1.44 reduced) for the linear fit and 5.02 (1.26 reduced) for the constant one. In addition, taking into account the symmetry of the ellipse, a parabolic fit was also done, which gives a χ^2 of 3.26 (1.63 reduced). It can therefore be concluded that the three models are statistically compatible with the data.

5 Conclusions

5.1 Solar meridian transit

The observations of the meridian transits confirmed that the Clementine Gnomon remains an incredible instrument, capable of providing measurements with a precision on the order of a few millimeters for positions and less than one second for times. The main complications are due to the non-ideality of the pinhole, which is affected by atmospheric agents ([[2]]), causing deformation of the solar image due to atmospheric turbulence. Other factors to be considered and analyzed more accurately in the future are: the different materials that make up the instrument, such as white marble, whose reflection and absorption coefficients should be studied to obtain more precise measurements, as well as the uncertain orientation of the meridian line in the North-South direction. The most important factor is the need for good weather conditions in order to see the solar image and thus obtain data that one can work with (this is not always

the case, in April there were only 2-3 observations).

5.2 LDF

As shown before, the pinhole has proven to be a useful instrument beyond its original purpose. In fact, using modern technologies, it is possible to extend the precision beyond our original expectations, being limited only by the atmosphere and the camera systematics.
In the future, it will be possible to increase the precision by studying the camera's flat field, the statistical properties and the characteristic frequencies of atmospheric and local seeing.

5.3 Photodiode measurements

These preliminary results showed that a photodiode can be a useful instrument to obtain a better understanding of local seeing, in order to achieve more precise measurements. Showing, or not, if exists some correlation between b and the position of the ellipse and the external temperature is the first step to have a better comprehension of the local seeing and its effect on the measures. Obviously, there were also many issues that need to be solved in order to increase the precision on these kind of measurements, since, as can be seen, it's not very high: first of all, the Arduino UNO is not the ideal device to obtain measurements, because of the interactions during the measurements that compromise their quality. Then, for future measurements, it would be ideal to have a new photodiode able to save the data on its own memory or that can be continuously connected to a file without the oscillation problem. Moreover, the future photodiode should also have high resolution, in order to increase precision for future measurements. Of course, these results are not definitive, but they are the first step in the study of noise at the Clementine Gnomon.

References

[1] Rogerson, J.B. (1959) 'The solar limb intensity profile.', The Astrophysical Journal, 130, p. 985. Available at: doi:10.1086/146787;

[2] Sigismondi, C. (2011) Lo Gnomone Clementino: Astronomia Meridiana in Chiesa Dal '700 AD oggi, arXiv.org. Available at: https://arxiv.org/abs/1106.2498;

[3] Menzel, Donald H., Il Nostro Sole, Faenza Editrice (1981), pp. 205–228;

[4] RAPONI, A. et al. (2013) 'Eclipses, solar limb darkening function and diameter measurements: Toward a unified approach', International Journal of Modern Physics: Conference Series, 23, pp. 432–436, available at: doi:10.1142/s2010194513011719;

[5] Link to temperature maps of Rome from Meteo Blue.